Catalysis Today 328 (2019) 230–234

Contents lists available at ScienceDirect

Catalysis Today

journal homepage: www.elsevier.com/locate/cattod

New insight into zinc oxide doped with iron and its exploitation to pollutants abatement

Maria Cristina Paganini, Alice Giorgini, Nuno P.F. Gonçalves, Chiara Gionco, Alessandra Bianco Prevot, Paola Calza*

Department of Chemistry, Università di Torino, Torino, Italy

ARTICLE INFO

Keywords:
Iron doping
Zinc oxide
Pollutant abatement
Ketoprofen

ABSTRACT

This study aims to investigate how the photocatalytic efficiency of zinc oxide can be improved by introducing doping species into its crystal lattice. New materials based on zinc oxide doped with iron, have been synthesized using different methods, characterized and tested toward the abatement of selected organic molecules. The different synthetic strategies followed comprised sol-gel, precipitation and hydrothermal processes, in order to identify which one is capable of guaranteeing the best photocatalytic performances.

The photoactivity of the new semiconductors was firstly tested using phenol as a model molecule subjected to irradiation under UV-A light. Phenol abatement is particularly favoured when using ZnO prepared via hydrothermal method and doped with iron at 0.5%. These materials were then tested toward the elimination of ketoprofen, an emerging pollutant substance, from water and real wastewater. Ketoprofen and its transformation products are completely abated within 30 min in pure water or in 1 h in wastewater.

1. Introduction

Heterogeneous photocatalysis could play a fundamental role in the degradation of recalcitrant organic molecules present in environmental matrices. So, over the years a lot of research has been devoted to the development of semiconductor materials that could be applied to the purification of water. Among the semiconductor oxides, titanium dioxide and zinc oxide seem promising candidates.

Transition metal doping is one of the best-known strategies for improving the photocatalytic activity of a semiconductor, as these elements are able to modify the oxide band structure, morphology and particle size. When added in proper quantities, the metallic sites act as traps for the photoproduced charges, so increasing the charge transfer and reducing the extent of charge recombination [1]. Moreover, the doping with metals of d block solves the problem related to photocorrosion of zinc oxide which becomes more stable and thus more appealing to be used in wastewater treatment [2].

The positive role of transition metal doping is expressed through the introduction of additional energy levels inside the oxide band gap. Furthermore, the addition of transition metals changes the chemical surrounding of Zn^{2+} ions, induces reticular distortions and increases the fraction of defects. In particular, the oxygen vacancies, if present in optimal concentrations, can act as traps for the electrons and guarantee a better efficiency in the electrons /holes charge separation [3].

The present work aims to develop new photoactive materials, potentially applicable to water treatment. Several synthetic strategies, not expensive and easy to perform, have been investigated, aimed to achieve the development of materials with enhanced photocatalytic performances. Among all the possible doping we have chosen iron, a transition metal that is easy to find and very abundant on the earth's crust. Also zinc oxide is particularly easy to find, so the Fe/ZnO system can be a sustainable and economical photocatalyst. We assessed how the photocatalytic efficiency of the zinc oxide can be improved by introducing iron in its reticular structure. The effect of the type of synthetic process (sol-gel, precipitation and hydrothermal methods) and of the dopant concentration (from 0.5% to 3%) on the efficiency of photocatalysis was studied.

2. Materials and methods

2.1. Materials

The precursors and reagents used in the synthesis of new materials and in subsequent analyzes for the evaluation of their photocatalytic activity, were purchased by Sigma-Aldrich. Suspensions and standard solutions were prepared in MilliQ water.

* Corresponding author at: Università di Torino, via P. Giuria 5, 10125 Torino, Italy.
E-mail address: paola.calza@unito.it (P. Calza).

https://doi.org/10.1016/j.cattod.2018.10.054
Received 27 June 2018; Received in revised form 4 September 2018; Accepted 22 October 2018
Available online 28 October 2018
0920-5861/ © 2018 The Authors. Published by Elsevier B.V. This is an open access article under the CC BY-NC-ND license (http://creativecommons.org/licenses/BY-NC-ND/4.0/).

The real wastewater samples were provided by SMAT S.p.A. (Società Metropolitana Acque Torino, Italy) and were sampled at the wastewater treatment facility of Castiglione Torinese (Italy) on 27 October 2017. The samples used in this work were obtained from the outflow of the primary clarifier tank (hereafter, Primary sample). Real samples were used after a rough pre-filtration step, carried out through a grade 1 qualitative filter paper (Whatman) to remove large suspended solids and filtered using a hydrophilic 0.45 μm filter Sartolon Polyamide by Sartorius Biolab.

2.2. Synthesis procedures

2.2.1. Synthesis via sol-gel (SG)

Zinc acetate is solubilized in 250 mL of deionized water; the desired stoichiometric amount of $Fe(NO_3)_3$ is added to the solution together with 5 g of citric acid. The solution is subjected to magnetic stirring and is kept for 6 h in a hot water bath at 80 °C, in order to favor the gel formation [4]. The acidic pH favors the hydrolysis process and therefore the gelation. The beaker containing the gel is placed in an oven at 70 °C for two days, in order to promote drying and obtaining the xerogel. This phase is followed by a further heat treatment which involves calcining in a muffle at 500 °C for 2 h.

2.2.2. Synthesis via precipitation (P)

The precipitation method is a simple and versatile approach for the synthesis of semiconductor materials; it is cheap, does not require complex experimental conditions [5]. The solution of the precursors, named A, is obtained by adding 2.2 g of zinc acetate dihydrate and the stoichiometric amount of $FeCl_3$ to 160 mL of deionized water. 80 mL of ethanol are then added to solution A and the system is kept under magnetic stirring for 1 h in order to promote the solubilization of inorganic salts. Then, 160 mL of NaOH 1 M (solution B) are added drop by drop to the solution A. The precipitate is left to rest for two days, recovered by filtration and dried in an oven at 70 °C. The powder is finally calcined at 300 °C for 30 h [6].

2.2.3. Synthesis via hydrothermal method (H)

The doping agent ($FeCl_3$), in the desired percentage, was added to 20 mL of $Zn(NO_3)_2{\cdot}6H_2O$ 1M solution, and the resulted solution was kept under stirring. After complete dissolution, a solution of NaOH 4M was added dropwise until reaching the pH value of 10. The solution was transferred to a 100 mL Teflon-lined autoclave, filled with water until complete 50 mL, and the autoclave was kept at 175 °C for 15 h. The resulting precipitated product was washed with water and recovered by centrifugation (6000 rpm for 10 min), repeating the procedure 2 times. After dried at 70 °C during the night, the powder was homogenized using a mortar and pestle.

2.3. Methods

2.3.1. XRD

X-rays powder diffraction (XRPD) patterns were recorded using a PANalytical PW3040/60 X'Pert PRO MPD, Lissone (MI) Italy (45 kV, 40 mA) with a copper K_α radiation source (0.15418 nm). Samples were scanned continuously in the 2θ range between 10° and 100°. The X'Pert High-Score software was used to identify the mineral phases present in the samples.

2.3.2. DR-UV-Vis

The UV–vis absorption spectra were recorded using a Varian Cary 5000 spectrophotometer, coupled with an integration sphere for diffuse reflectance studies (DRS) and a Carywin-UV/scan software. A sample of PTFE with 100% reflectance was used as reference.

2.3.3. Photocatalytic degradation experiments

The irradiation experiments were carried out in magnetic stirred Pyrex glass cells, filled with 5 mL of model molecule (20 mg/L) and catalyst (1000 mg/L or 400 mg/L). Samples were irradiated for different times (from 5 min to 120 min) using a PHILIPS cleo 6 × 15 W TL-D Actinic BL with maximum emission wavelength at 365 nm. The UV integrated irradiance on the cells in the 290–400 nm range wavelengths was 90 ± 2 Wm^{-2} (measured with a CO.FO.MEGRA (Milan, Italy) power-meter). After irradiation, samples were filtered through a 0.45 μm filter and analyzed with the proper analytical technique.

Ketoprofen degradation was also performed in effluent wastewater provided by SMAT S.p.A. (Turin, Italy). Total organic carbon measures on wastewater matrix allowed to determine a concentration of organic component equal to 9.7 mg/L and inorganic carbon 68.4 mg/L. The organic nitrogen measures allowed to determine of 31.3 mg/L of total nitrogen.

2.3.4. HPLC/UV

The concentrations of phenol and ketoprofen were measured through a YL9300 HPLC system equipped with a YL9330 Column Compartment and a YL9150 autosampler. The column was a RP C18 column (LiChroCART®, Merck, 12.5 cm × 0.4 cm; 5 m packing). Phenol was analyzed using acetonitrile and phosphoric acid solution (1×10^{-2} M) at pH 2.8 (10: 90% v/v) as eluent at a flow rate of 1 mL/min and UV detector set at 220 nm. Ketoprofen was analyzed using as eluent acetonitrile and phosphoric acid solution (1×10^{-2} M) at pH 2.8 (35: 65% v/v) at a flow rate of 1 mL/min and UV detector set at 260 nm.

2.3.5. HPLC/MS

Samples were analyzed by HPLC/MS Shimadzu UFLC equipped with a Nexera XR, LC-20AD XR pump and a UV–vis detector SPD-M20A. Injection volume was 10 μL and flow rate 0.4 mL/min using a column Phenomenex Luna C18 50 × 2 mm, 2.5 μm and a gradient mobile phase composed of acetonitrile/water was: 0 min, 5/95; 5 min 0 /100; 7 min, 0/100. A 3200 Q Trap Sciex mass spectrometer equipped with an atmospheric pressure interface and an ESI ion source was used. Samples were analyzed using ESI negative mode operating in full-scan mode between 50 and 300 *m/z* range.

2.3.6. Total organic carbon

Total organic carbon (TOC) and total nitrogen (TN) were measured using a Shimadzu TOC-5000 analyzer (catalytic oxidation on Pt at 680 °C). The calibration was performed using standards of potassium phthalate.

2.3.7. Iron leaching

The determination of iron released in solution was evaluated by a spectrophotometric procedure. After irradiation, the 1000 ppm suspension of catalyst was filtered with hydrophilic PTFE Millex-LCR filters (0.45 mm pore diameter). The iron released was determined by adding ascorbic acid (0.5 mM) to reduce the Fe(III) to Fe(II) and complexing the Fe(II) with *o*-phenanthroline (5 mM). The absorption of the iron-thiocyanate complex was determined at 510 nm. Spectrophotometric analyses were performed using a Varian CARY 100 Scan double-beam UV–vis spectrophotometer, using quartz cuvettes with 10 mm path length.

3. Results and discussion

3.1. Materials characterization

3.1.1. Iron doped materials

Fig. 1 shows the diffraction patterns of pure and doped samples. All the diffractograms present the reflections typical of wurtzite ZnO (ICDD 01-089-7102 reference pattern). None of the doped samples show reflections related to other phases, such as iron oxides, α-Fe_2O_3 or γ-Fe_2O_3 [7]. This means either that the iron ions entered the structure of zinc oxide substitutionally or that the iron oxide phases are too small to

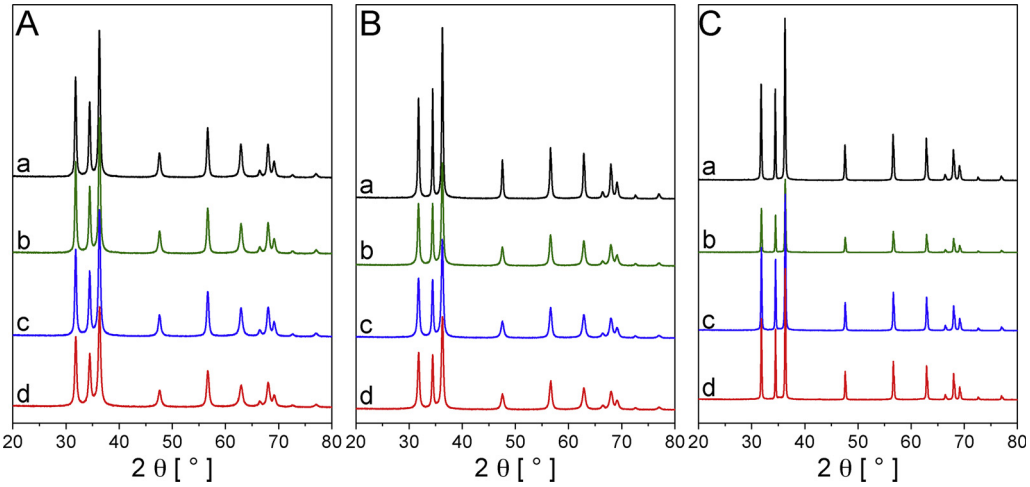

Fig. 1. XRD patterns of bare (trace a) and Fe-doped ZnO with different iron contents: 0.5% (trace b), 1% (trace c) and 3% (trace d). Samples were prepared via sol-gel (panel A), precipitation (panel B) and hydrothermal methods (panel C).

be detected with the XRD analysis.

The addition of iron changes the average crystalline size of ZnO, calculated using the Debye-Scherrer equation, as reported in Table 1. Indeed, the XRD peaks of the doped samples result broadened with respect to the pattern of the bare oxide. This phenomenon is quite known in literature, and it is attributable to the fact that the presence of the dopant ion prevents the growth of crystallites, favoring instead nucleation. The hydrothermal synthesis leads to the formation of materials with a higher degree of crystallinity (average crystallite size around 100–150 nm) as evidenced also by the comparison of pure ZnO samples for the different synthesis methods reported in the supporting information (Fig. S1), while the sol-gel and precipitation synthesis both form crystallites with an average size around 20 nm.

Fig. 2 shows DR-UV–vis spectra for all samples. It is clear from the spectra, and from the energy gap values calculated using the Tauc plot reported in Table 1, that the addition of iron does not affect dramatically the fundamental edge transition due to the excitation between the material's valence and conduction bands. On the other hand, the addition of iron leads to the formation of an additional absorption shoulder, that can be related to iron states. The intensity of this band is highly dependent on the material's synthesis, the most intense being the one obtained with the precipitation method. Fig. S2 reports the comparison of the DR spectra for the samples containing 3% of iron obtained with the different synthesis. Fig. S2 highlight the presence of two intra-band features. The first one, centered at 420 nm, was assigned for the analogous system Fe-TiO_2, to the charge transfer between Fe^{3+} states and the oxide conduction band. This band is present in the samples prepared with the precipitation and the hydrothermal methods, while it was absent in the samples prepared through the sol-gel method. The second feature, represents the main absorption in the visible region and it is centered at 500 nm. This band has been attributed in the past to "on-site" transitions (d-d transitions on the Fe^{3+} ion) or to inter-site transitions (between two Fe^{3+} ions) [8–11].

Table 1
Average size of crystallites (d), energy gap values (E_{BG}) and calculated kinetic constant (phenol 20 mg/L, catalyst 1000 mg/L) for pure and doped zinc oxide samples.

Synthesis	% dopant	d [nm][a]	E_{BG} [eV][b]	k, min^{-1}
SG	**0**	21 ± 7	3.24	0.04
	0.5	20 ± 5	3.21	0.011
	1	21 ± 5	3.23	0.0048
	3	14 ± 4	3.24	0.0036
P	**0**	37 ± 5	3.27	0.03
	0.5	19 ± 6	3.27	0.044
	1	19 ± 5	3.27	0.025
	3	18 ± 4	3.25	0.026
H	**0**	143 ± 30	3.28	0.058
	0.5	112 ± 17	3.27	0.171
	1	91 ± 13	3.27	0.123
	3	120 ± 14	3.25	0.035

[a] As calculated from the Scherrer equation.
[b] As obtained from the Tauc plot.

3.2. Photoactivity tested on a probe molecule

3.2.1. Influence of the synthesis method

The photocatalytic activity of all synthesized materials was evaluated by using phenol as a model molecule in MilliQ water. Fig. 3 shows the degradation curves obtained by irradiating the probe molecule in the presence of pristine or doped zinc oxide, at different dopant concentrations produced through hydrothermal method, while data obtained from sol-gel and precipitation methods are plotted in Figs. S3 and S4, respectively.

For a complete view, we report in Table 1 the kinetic constants values calculated from phenol degradation curves for all synthesized materials. Materials prepared via sol-gel method exhibit a poor activity and permit to abate only a small percentage of phenol (from 20 to 40% after 2 h of irradiation, see Fig. S3), while oxides produced through hydrothermal method were the most efficient.

The materials prepared via hydrothermal method allowed to degrade the probe molecule with kinetic constants which are greater of one order of magnitude compared to those characteristics of the precipitated powders. This phenomenon could be probably due to the higher degree of crystallinity of the former as pointed out by the XRD patterns. Iron leaching was tested as well on doped materials prepared via hydrothermal method and, in all case, is negligible.

3.2.2. Doping effect

Data collected in Table 1 allowed to assess that iron doping induced an enhancement in the phenol degradation rate compared to pristine ZnO, with SG method only exception. Results obtained for materials prepared via hydrothermal or precipitation method show that ZnO doped with the lowest concentration of iron, namely 0.5%, promotes the phenol degradation with the highest kinetics, while the photoactivity is reduced as the dopant concentration increases.

In fact, the sample containing the lowest dopant concentration ensures the complete elimination of the phenol after only 30 min of irradiation with Fe(0.5%)-ZnO-H (see Fig. 3) or 60 min with Fe(0.5%)-ZnO-P (see Fig. S4). Instead, as the amount of iron increases, the

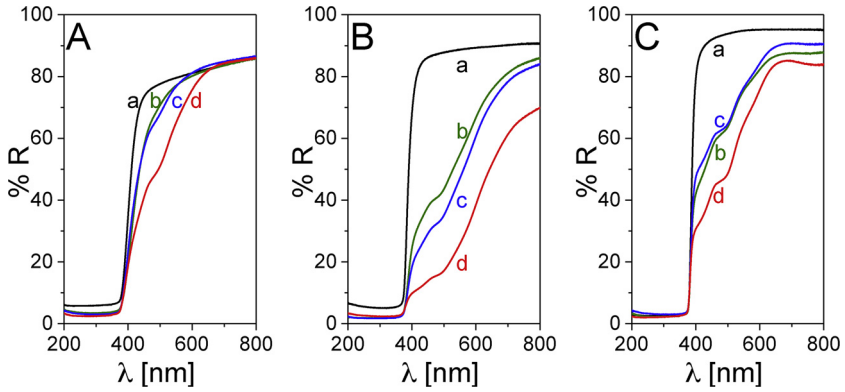

Fig. 2. DR spectra for bare (trace a) and Fe-doped ZnO with different iron contents: 0.5% (trace b), 1% (trace c) and 3% (trace d). Samples were prepared via sol-gel (panel A), precipitation (panel B) and hydrothermal (panel C) methods.

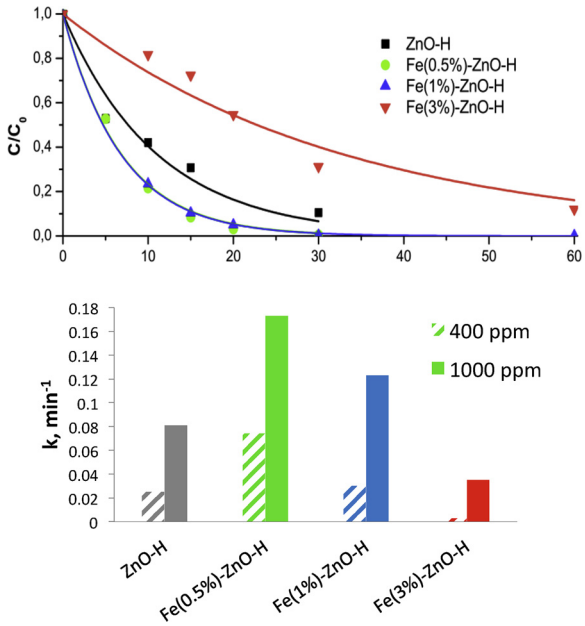

Fig. 3. Phenol degradation (20 mg/L) under UV-A in the presence of (top) Fe-ZnO-H 1000 mg/L and (bottom) kinetic constants of phenol abatement in the presence of different catalysts at 400 mg/L and 1000 mg/L.

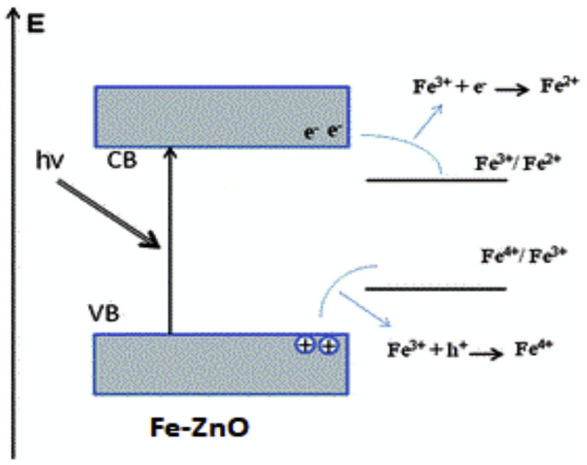

Scheme 1. Energetic levels for Fe-doped ZnO.

performances are reduced and become lower than those of the pristine semiconductor; less than 90% of the initial phenol was eliminated in 1 h when the highest concentration of dopant is used.

For comparison purpose, the kinetic constants for all materials obtained via hydrothermal method are plotted in Fig. 3 (bottom), where two catalysts concentration (1000 mg/L or 400 mg/L) were considered. As expected, although the values of the kinetic constants are reduced by decreasing the photocatalyst concentration, the order of reactivity already observed for the materials is maintained.

To explain the reasons for such experimental evidences, it is necessary to consider the role played by the dopant within the crystalline lattice of zinc oxide. It is well-known that electron/hole recombination limits the photocatalytic efficiency and has therefore to be prevented. Iron acts as a surficial trap for the photogenerated charges generated and, therefore, prevents or in any case reduces the electrons/holes recombination [12]. The possibility for Fe^{3+} to undergo redox reactions introduces two discrete levels of energy into the oxide band gap, as shown in Scheme 1.

The oxide conduction band has an energy close to the redox potential of the Fe^{3+}/Fe^{2+} pair and Fe^{3+} ion can, therefore, behave as a scavenger for the photogenerated electrons and be reduced to Fe^{2+}. Fe^{2+} ion can then easily transfer an electron to the oxygen adsorbed on the semiconductor surface, so favoring the formation of the superoxide anion radical, as described in reactions (1) and (2).

$$Fe^{3+} + e_{CB}^{-} \rightarrow Fe^{2+} \quad (1)$$

$$Fe^{2+} + O_{2(ads)} \rightarrow Fe^{3+} + O_2^{-\bullet} \quad (2)$$

Fe^{3+} ion can also act as a capture center in the valence band. The resulting Fe^{4+} combines with the surface hydroxyl groups to produce the OH radicals [13].

$$Fe^{3+} + h_{VB}^{+} \rightarrow Fe^{4+} \quad (3)$$

$$Fe^{4+} + OH^{-} \rightarrow Fe^{3+} + OH^{\bullet} \quad (4)$$

Therefore, the enhanced degradation of phenol obtained following iron doping could be attributed to the increased production of reactive oxygen species, described through reactions (1)–(4).

However, an excessive addition of dopant inhibits the degradation process. The order of photoactivity of the materials is modified for the highest concentrations of doping. In this case, pure oxide has the greatest photoactivity, attributable to an increase in electron/hole recombination with a consequent reduction in the performance of doped semiconductors [14]. In fact, a high concentration of iron reduces the degree of crystallinity of the solid and increases the fraction of reticular defects, which represent preferential centers where electron/hole recombination could occur. From the collected data it can be inferred that 3% of dopant is enough to favor charge recombination rather than charge separation. However, some studies showed that the highest photoactivity is guaranteed by the materials containing the highest doping concentrations [5].

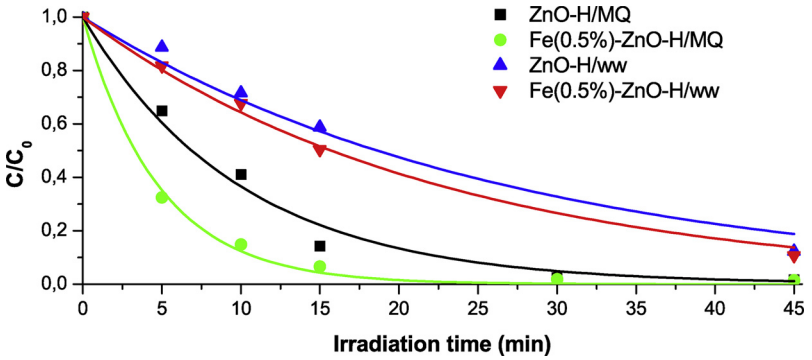

Fig. 4. Ketoprofen degradation (20 mg/L) in the presence of 1000 mg/L of catalyst in Milli-Q (MQ) water and wastewater (ww).

3.2.3. *Phenol transformation products*

The evolution over time of the main transformation products (TPs) arose during phenol degradation was followed as well. The formation of catechol, hydroquinone and resorcinol occurred in all cases, in agreement with literature data [15–17], and their evolution profiles are plotted in Fig. S6.

Doping with the lowest percentages of iron allows the abatement of the intermediate in times shorter than those necessary for pristine oxide. The disappearance of the intermediate is already observed at 30 min of irradiation with ZnO doped at 0.5% and 1%. Instead, 1 h of irradiation is required for the 3% Fe-doped material. In particular, catechol maximum concentration is achieved, for all the materials, at short irradiation times (10 min of irradiation for pristine ZnO and ZnO doped with the lowest concentrations of iron, and 15 min for ZnO doped at 3%). Similarly, to what has been observed for catechol, the disappearance kinetics of hydroquinone is slower for samples characterized by the highest doping content.

3.3. *Application to emerging contaminant degradation*

The best performing material, namely Fe(0.5%)-ZnO-H, was also tested toward the abatement of ketoprofen, a contaminant of emerging concern, and the degradation profiles are shown in Fig. 4. Analyzing data in MilliQ water, Fe(0.5%)-ZnO-H permits to achieve the complete degradation of ketoprofen in 20 min, while ZnO-H requires 45 min.

The effect of matrix composition was assessed as well after added spiking a real wastewater with ketoprofen and then by studying the drug degradation. The high organic load, combined with the presence in the real matrix of inorganic ions, is the reason why the degradation curves go to zero more slowly than those acquired in MilliQ water [18]. Even if rates are slightly decreased, all materials are able to completely abate the molecule within 1 h of irradiation.

The formation of transformation products (TPs) was assessed too and their evolution profiles are plotted in Fig. S7 (ZnO-H) and S8 (Fe (0.5%)-ZnO-H). Ketoprofen transformation involved in all cases the formation of several hydroxylated derivatives, in a close analogy with TPs already detected during the treatment with titanium dioxide [19] and in surface water [20]. In the presence of Fe(0.5%)-ZnO-H, all TPs are formed within few minutes (maximum at 5 min) and completely disappeared within 30 min, while with ZnO-H the evolution profiles are delayed and a longer irradiation time is required to achieve the complete TPs abatement.

4. Conclusions

The sol-gel synthesis led to the design of materials with limited photocatalytic activity, while the most promising synthesis procedures were those obtained via precipitation and hydrothermal processes. Among the various strategies of investigated synthesis, the hydrothermal method proved to be the most advantageous in the development of materials characterized by excellent photocatalytic performances. The initial objective of increasing the photoactivity of zinc oxide is reached by using doping with iron at low concentrations (0.5%), for which a clear improvement is observed in the abatement of the model molecule. The transition metal ions, if present in suitable quantities, act as surface traps for the photoinduced charges and reduce e^-/h^+ recombination. Conversely, when present at high concentrations, charge recombination prevails on charge separation, so affecting (and decreasing) the degradation performance.

From the obtained results it is possible to deduce that the synthesized materials are efficient, not only in the elimination of the phenol, but also in the removal of the degradation intermediates. All the materials synthesized by hydrothermal method are able to completely degrade the aromatic products formed by the degradation of phenol (catechol, hydroquinone and resorcinol) within 2 h of irradiation.

The best performing materials have also been successfully applied for the abatement of ketoprofen in real wastewater.

Acknowledgements

This work is part of a project that has received funding from the European Union's Horizon 2020 research and innovation programme under the Marie Skłodowska-Curie Grant Agreement No 765860 (AQUAlity). We acknowledge support from MCA-H2020-RISE (MAT4TREAT, no. 645551) as well.

References

[1] R. Saleh, N.F. Djaja, Spectrochim. Acta A. Mol. Biomol. Spectrosc. 130 (2014) 581–590.
[2] M. Samadi, M. Zirak, A. Naseri, E. Khorashadizade, A.Z. Moshfegh, Thin Solid Films 605 (2016) 2–19.
[3] Y. Lu, Y. Lin, D. Wang, L. Wang, T. Xie, T. Jiang, Nano Res. 11 (4) (2011) 1144–1152.
[4] W. Bousslama, H. Elhouichet, M. Férid, Optik 134 (2017) 88–89.
[5] R. Saleh, N.F. Djaja, Superlattices Microstruct. 74 (2014) 217–233.
[6] E. Cerrato, C. Gionco, M.C. Paganini, E. Giamello, J. Phys. Condens. Matter 29 (2017) 444001.
[7] H. Liu, J. Yang, Y. Zhang, L. Yang, M. Wei, X. Ding, J. Phys. Condens. Matter 21 (14) (2009) 145803–146001.
[8] K.C. Christoforidis, A. Iglesias-Juez, S.J.A. Figueroa, M. Di Michiel, M.A. Newton, M. Fernández-García, Catal. Sci. Technol. 3 (2013) 626–634.
[9] T. Umebayashi, T. Yamaki, H. Itoh, K. Asai, J. Phys. Chem. Solids 63 (2002) 1909–1920.
[10] J. Zhang, X. Chen, Y. Shen, Y. Li, Z. Hu, J. Chu, Phys. Chem. Chem. Phys. 13 (2011) 13096–13105.
[11] J. Zhu, W. Zheng, B. He, J. Zhang, M. Anpo, J. Mol. Catal. A Chem. 216 (2004) 35–43.
[12] C. Adàn, A. Bahamonde, M. Fernàndez-Garcia, A. Martìnez-Arias, Appl. Catal. B 72 (2007) 11–17.
[13] M. Ba-Abbad, A.A.H. Kadhum, A.B. Mohamad, M.S. Takriff, Chemosphere 91 (2013) 1604–1611.
[14] V.C. Srivastava, P. Chandra, Ind. Eng. Chem. Res. 52 (2013) 17790–17799.
[15] T.T.T. Dang, S.T.T. Le, D. Channei, W. Khanitchaidecha, A. Nakaruk, Res. Chem. Intermed. 42 (2016) 5961–5974.
[16] Z. Guo, R. Ma, G. Li, Chem. Eng. J. 119 (2006) 55–59.
[17] K.I. Okamoto, Y. Yamamoto, H. Tanaka, M. Tanaka, A. Itaya, Bull. Chem. Soc. Jpn. 58 (1985) 2015–2022.
[18] S. Carbonaro, M.N. Sugihara, T.J. Strathmann, Appl. Catal B: Environ. 129 (2013) 1–12.
[19] C. Martínez, S. Vilari ˜no, M.I. Fernández, J. Faria, L.M. Canle, J.A. Santaballa, Appl. Catal. B 142–143 (2013) 633–646.
[20] A. Jakimska, M. Śliwka-Kaszyńska, J. Reszczyńska, J. Namieśnik, A. Kot-Wasik, Anal. Bioanal. Chem. 406 (2014) 3667–3680.